Magneto-optical measurements of hysteresis loop and anisotropy energy constants on amorphous Tb_xFe_{1-x} alloys

Cite as: Journal of Applied Physics **60**, 346 (1986); https://doi.org/10.1063/1.337651
Submitted: 06 January 1986 . Accepted: 13 March 1986 . Published Online: 14 August 1998

P. Wolniansky, S. Chase, R. Rosenvold, M. Ruane, and M. Mansuripur

Magneto-optical measurements of hysteresis loop and anisotropy energy constants on amorphous Tb_xFe_{1-x} alloys

P. Wolniansky, S. Chase, R. Rosenvold, M. Ruane, and M. Mansuripur
Boston University, College of Engineering, 110 Cummington Street, Boston, Massachusetts 02215

(Received 6 January 1986; accepted for publication 13 March 1986)

Measurements of the Kerr magneto-optic effect, coercivity, and anisotropy energy constants are performed in a magneto-optical system that combines the Kerr rotation angle and ellipticity to enhance the strength of the signal. The temperature dependence of the polar Kerr effect is compared with the magnetization of the iron subnetwork in the mean-field approximation and good agreement is obtained in all cases. Coercivity is found to be a strong function of the sweeping frequency and the saturating field and the results are found to be in qualitative agreement with the magnetization reversal model based on the existence of initial nuclei in a saturated film and the subsequent growth of these nuclei under a reverse field. Finally, perpendicular magnetic anisotropy energy is studied by magneto-optical techniques and the first two coefficients in the expansion of anisotropy energy in powers of the angle of deviation from the easy axis are determined.

I. INTRODUCTION

Amorphous rare-earth-transition metal alloys are now considered the most promising media for erasable optical data storage applications.[1-5] A better understanding of the magnetic, optical, and thermal properties of these media is therefore of the utmost significance. In this paper we report on magneto-optical measurements performed on Tb_xFe_{1-x} alloys, prepared by sputtering onto quartz substrates, and compare these results with theoretical models. We propose a minor modification to the standard magneto-optical detection system that can eliminate ellipticity from the MO signal and thus enhance the signal-to-noise ratio. A similar scheme has been proposed in the past which required the rather expensive Soleil–Babinet compensator. Our scheme which requires only a quarter-wave plate is described in Sec. II. Section III is devoted to hysteresis loop measurements; comparisons are made between the temperature dependence of the magneto-optical Kerr effect and the iron subnetwork magnetization derived from a mean-field theory. In Sec. IV we describe our results of anisotropy energy measurements and show that second-order terms must be included in the expression for uniaxial anisotropy energy in order to explain the data. The final section contains some concluding remarks.

II. MEASUREMENT SYSTEM

Figure 1 is a schematic diagram of the hysteresis loop tracer. The HeNe laser beam is linearly polarized in an arbitrary direction. The quarter-wave plate is used to eliminate ellipticity, and in the following discussion we assume that its fast axis has an angle ξ with the plane of incidence. The half-wave plate is used here to balance the amount of light between the two detectors and its fast axis has angle η with the plane of incidence. The polarizing beam splitter's axes are at 0° and 90° and the detectors have conversion factor α.

Let us define amplitude reflectivities $r_\parallel e^{j\phi_\parallel}$ and $r_\perp e^{j\phi_\perp}$ for the components of polarization that are parallel and perpendicular to the direction of incident polarization on the sample. Then if A is the effective amplitude of incident light, the reflected amplitude will be

$$\mathbf{A}_1(t) = Ar_\parallel \cos(\omega t + \phi_\parallel)\hat{a}_\parallel + Ar_\perp \cos(\omega t + \phi_\perp)\hat{a}_\perp, \quad (1)$$

where $\hat{a}_\parallel$ and $\hat{a}_\perp$ are unit vectors in the directions parallel and perpendicular to the direction of incident polarization. After passage through the $\lambda/4$ plate we will have

$$\begin{aligned}\mathbf{A}_2(t) = {} & [Ar_\parallel \cos(\omega t + \phi_\parallel)\cos\xi + Ar_\perp \\ & \times \cos(\omega t + \phi_\perp)\sin\xi\,]\hat{a}_x + [Ar_\parallel \sin(\omega t + \phi_\parallel) \\ & \times \sin\xi - Ar_\perp \sin(\omega t + \phi_\perp)\cos\xi\,]\hat{a}_y, \quad (2)\end{aligned}$$

where $\hat{a}_x$ and $\hat{a}_y$ are along the axes of the $\lambda/4$ plate. The passage through the $\lambda/2$ plate has the effect of rotating the components of polarization with respect to the axis of the plate. Equation (2) will thus hold for the light amplitude after $\lambda/2$ plate provided that $\hat{a}_x$ is interpreted as an axis which has an angle $2\eta - \xi$ with the plane of incidence. This beam is now divided by the PBS between the photodiodes. It is not difficult to show that the sum and the difference of the photodiode outputs are given by

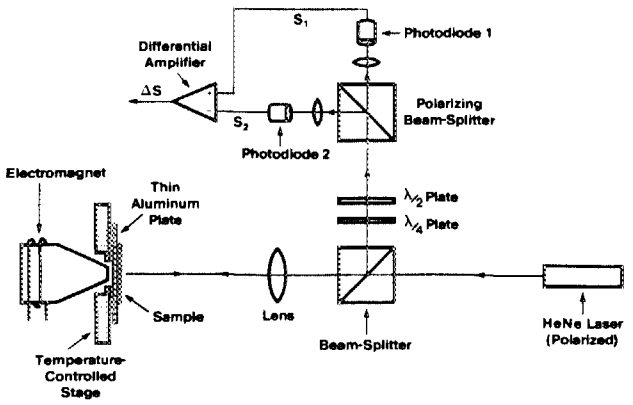

FIG. 1. Schematic diagram of the measurement system.

 0021-8979/86/130346-06$02.40

$$\sigma = S_1 + S_2 = \tfrac{1}{2}\alpha A^2(r_\parallel^2 + r_\perp^2), \tag{3}$$

$$\begin{aligned}\Delta S = S_1 - S_2 = \tfrac{1}{2}\alpha A^2[&(r_\parallel^2 - r_\perp^2)\cos 2\xi \cos(4\eta - 2\xi) \\ &+ 2r_\parallel r_\perp \cos(\phi_\parallel - \phi_\perp)\sin 2\xi \cos(4\eta - 2\xi) \\ &+ 2r_\parallel r_\perp \sin(\phi_\parallel - \phi_\perp)\sin(4\eta - 2\xi)].\end{aligned} \tag{4}$$

Now, if we set $\xi = 45°$, Eq. (4) becomes

$$\Delta S = \alpha A^2 r_\parallel r_\perp \sin(\phi_\parallel - \phi_\perp - 4\eta). \tag{5}$$

Switching the magnetization of the sample has the effect of replacing $\phi_\perp$ by $\phi_\perp + 180°$ in the above equation. Thus, upon reversing the magnetization, ΔS will change sign. The net signal at the output of the differential amplifier is then $\delta = 2\Delta S$. Normalizing this with the sum of S_1 and S_2 as given by Eq. (3) we obtain

$$\frac{\delta}{4\sigma} = \frac{r_\parallel r_\perp \sin(\phi_\parallel - \phi_\perp - 4\eta)}{r_\parallel^2 + r_\perp^2}. \tag{6}$$

η can thus be set to maximize the signal in Eq. (6). This happens when $\eta = \eta_0 = (\phi_\parallel - \phi_\perp + 90°)/4$. If η is changed from η_0 by 22.5° the signal completely disappears.

It is thus observed that the system of Fig. 1 can enhance the signal-to-noise ratio by eliminating the phase factor $(\phi_\parallel - \phi_\perp)$. The same thing can be achieved by replacing the $\lambda/4$ plate with an adjustable phase plate in a straightforward manner[6] but the adjustable plates are usually much more expensive than the $\lambda/4$ plates. Without either the $\lambda/4$ plate or the adjustable phase plate it can be shown that the signal is given by

$$\delta/4\sigma = r_\parallel r_\perp \cos(\phi_\parallel - \phi_\perp)\sin(4\eta)/(r_\parallel^2 + r_\perp^2), \tag{7}$$

in which $\eta = 22.5°$ is optimum and the signal is lower than that given in Eq. (6) by a factor of $\cos(\phi_\parallel - \phi_\perp)$.

For the media of interest in this work it is generally true that $r_\perp \ll r_\parallel$. Under this condition the system of Fig. 1 will measure $\delta/4\sigma \simeq r_\perp/r_\parallel$ which we will refer to as the enhanced Kerr rotation angle ($\hat{\theta}_k$). Without the $\lambda/4$ plate this system measures $\delta/4\sigma \sim (r_\perp/r_\parallel)\cos(\phi_\parallel - \phi_\perp)$. This latter quantity is the usual Kerr angle and will be referred to as θ_k. Figure 2 shows the results of measurements on $Tb_x Fe_{1-x}$ samples for several values of x. The symbol $\odot$ corresponds to θ_k while the symbol $\times$ corresponds to $\hat{\theta}_k$. Samples 1, 2, 3, and 4 are about 1000 Å thick and are measured through a 300-Å-thick glass overcoating layer. These are considered optically thick films and, in general, the amount of ellipticity for these samples is small. This is why the enhancement effect of the $\lambda/4$ plate is moderate. Samples 5 and 6, on the other hand, are quadrilayers with 300 and 150-Å-thick TbFe layers, respectively. The large amount of ellipticity for these samples has been converted into a useful signal by the quarter-wave plate, giving rise to a significant increase in the signal.

The detection scheme of Fig. 1 can obviously be used in magneto-optical disk systems to enhance the signal-to-noise ratio. The half-wave plate is not an essential part of the system and can be eliminated provided that the direction of incident polarization is initially adjusted with respect to the polarizing beam splitter.

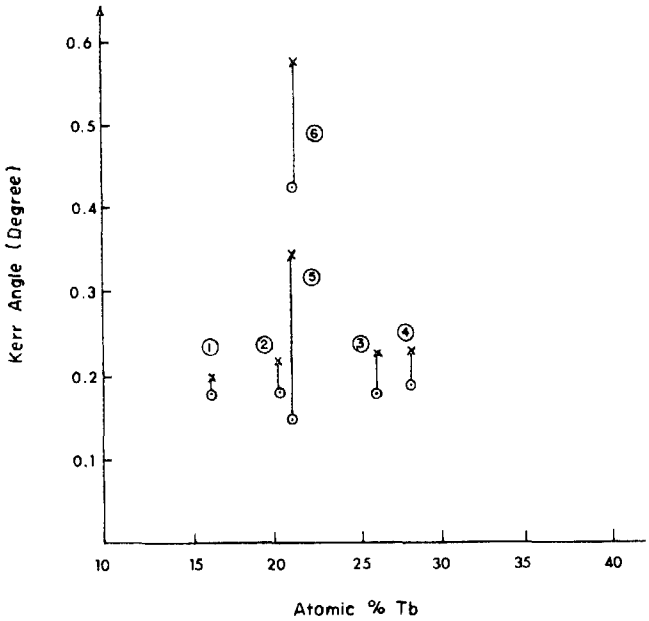

FIG. 2. Improvement in Kerr rotation angle as a result of eliminating ellipticity. The $\odot$ corresponds to regular Kerr effect θ_k, $\times$ to enhanced Kerr effect $\hat{\theta}_k$.

III. HYSTERESIS LOOP MEASUREMENTS

Figure 3 shows the measured values of θ_k, $\hat{\theta}_k$, and H_c (the coercivity) versus temperature for a 1000-Å-thick sample of $Tb_x Fe_{1-x}$ with $x = 28.3$ at. % as measured by x-ray fluorescence. The film was sputter deposited on a quartz substrate and *in situ* coated with 300 Å of SiO_2. The magnetic field is produced by an electromagnet driven by a sinusoidal current source of frequency $f = 0.1$ Hz and maximum current of 5.6 A. This corresponds to a sinusoidal field of the same frequency and $H_{max} = 3.2$ kOe at the TbFe layer. The laser was incident from the film side while the substrate was in thermal contact with a thin aluminum plate which was attached to the temperature controlled stage for uniform heat distribution on the sample. The hysteresis loops are

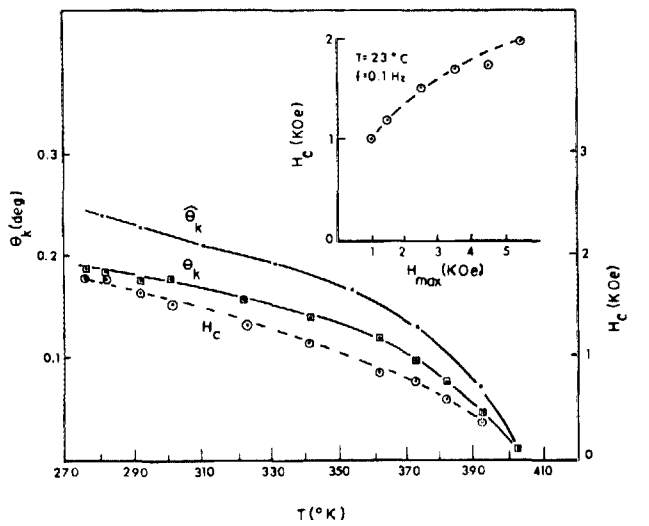

FIG. 3. Kerr rotation angle and coercivity vs temperature for a 975-Å-thick sample of $Tb_{28.3}Fe_{71.7}$. Sweep frequency = 0.1 Hz, $H_{max} = 3.2$ kOe. The inset shows the dependence of coercivity on H_{max}.

square at all temperatures up to the Curie point and the behavior of H_c versus temperature is characteristic of terbium-rich samples with no compensation point. Coercivity is found to be a strong function of the sweeping field frequency f and the maximum field amplitude H_{max}. The inset in Fig. 3 shows the dependence of H_c on H_{max} at $f = 0.1$ Hz. When H_{max} is below 2 kOe the strength of the signal (θ_k) is also reduced from its saturation value. Figure 4 shows the hysteresis loops at room temperature for various values of H_{max}. Qualitatively, their behavior is consistent with the explanation of magnetization reversal process based on the existence of initial nuclei in the saturated sample[7] and the phenomenon of magnetic after effect.[8] They also show that coercivity is not an inherent characteristic of the material and depends on the sweeping field characteristics as well.

The magneto-optic effect at red or near infrared wavelengths is believed to be the result of interaction between light and the transition metal subnetwork in rare-earth-transition metal (RE-TM) alloys. To a first-order approximation, the Kerr rotation angle θ_k is proportional to the magnetization of the TM subnetwork. Thus for TbFe samples we must have

$$M_{Fe}(T) = \beta\theta_k(T), \tag{8}$$

where β is the proportionality constant. The iron subnetwork magnetization can be calculated from the mean-field theory.[7] Figure 5 shows the results of this calculation for $(Tb_{29}Fe_{71})_{85}Ar_{15}$ (solid lines). The points indentified by $\times$'s in the figure represent $\theta_k(T)$ with the proportionality constant $\beta = 2500$. Although the agreement between the mean-field theory and the measured values of θ_k is extremely good, it is hardly conclusive. An independent test of the validity of the model is through the data obtained from measurements of saturation magnetization M_s versus temperature. The data of Mimura *et al.*[2] for a $Tb_{29}Fe_{71}$ sputter deposited sample is shown by the O's in Fig. 5. Their sample has a slightly higher Curie temperature and its magnetization lies above the $M_s(T)$ curve, obtained from the mean-field theory, in Fig. 5. The difference between the two samples could be attributed to the different amounts of impurity in the films, and in fact if the assumed amount of argon in the

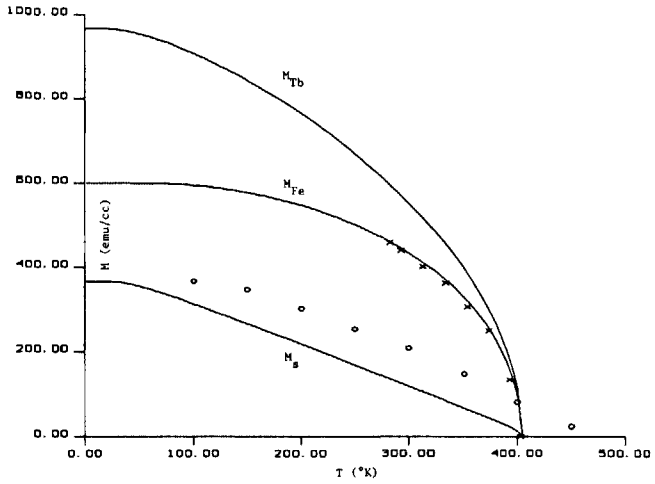

FIG. 5. Calculated and measured values of magnetization vs temperature for a terbium-rich sample.

sample is reduced from 15% to 5%, the mean-field model would give an exact match to the $M_s(T)$ data.

In Fig. 6 we show the results of hysteresis loop measurements on a $Tb_{20.3}Fe_{79.7}$ sample. Except for its composition, the sample is identical to the previous one. The experimental conditions are also the same. The hysteresis loops were square at all temperatures and the behavior of H_c vs T is characteristic of Fe-rich samples with a compensation point below room temperature. Figure 7 shows the net and the subnetwork magnetizations obtained from the mean-field theory for $(Tb_{20.5}Fe_{79.5})_{88}Ar_{12}$ composition (solid lines). The $\times$'s are θ_k data with $\beta = 2500$ and the O's are the M_s data of Mimura *et al.*[3] on a $Tb_{21}Fe_{79}$ sample. Again reducing the assumed amount of argon in the sample from 12% to 5% will give a better match to the M_s data.

Finally, hysteresis loops were obtained for a $(Tb_{17}Fe_{83})_{94}Cu_6$ sample which, except for its composition, is identical to the previous samples. The loops are characteristic of iron-rich samples but are not square. Lack of squareness is a consequence of the breakdown of magnetization into stripe domains as well as the existence of some in-plane magnetized regions. In any event, the coercivity cannot be

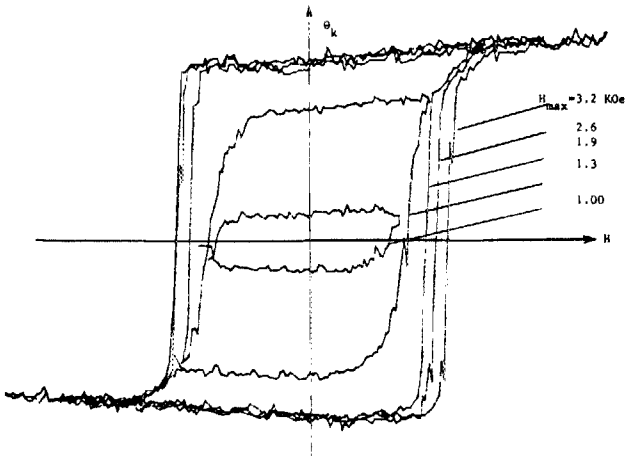

FIG. 4. Hysteresis loops at $T = 23$ °C and $f = 0.1$ Hz for a $Tb_{28.3}Fe_{71.7}$ sample. Different loops correspond to different values of H_{max}.

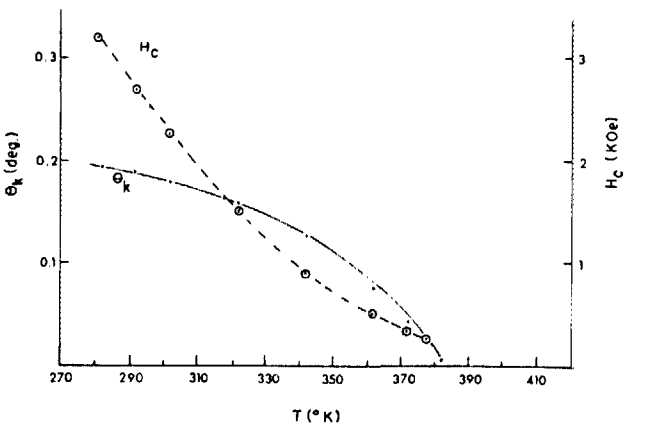

FIG. 6. Kerr rotation angle and coercivity vs temperature for a 1072-Å-thick sample of $Tb_{20.3}Fe_{79.7}$. Sweep frequency = 0.1 Hz, H_{max} = 3.2 kOe.

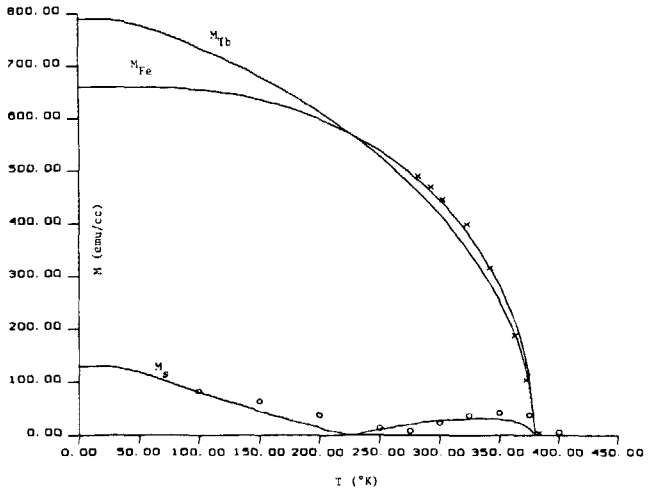

FIG. 7. Calculated and measured values of magnetization vs temperature for a sample with the compensation point at room temperature.

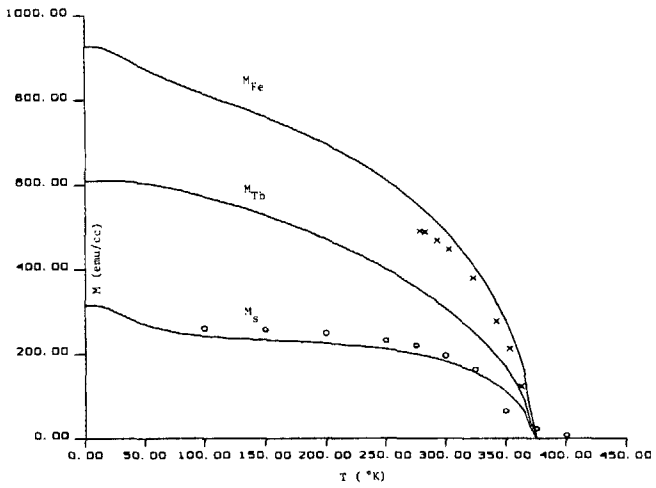

FIG. 9. Calculated and measured values of magnetization vs temperature for an iron-rich sample.

defined in a meaningful way for this sample and the Kerr angle θ_k must be measured at saturation, i.e., at $H = H_{max}$. The results are shown in Fig. 8. In order to compare the data with the mean-field model predictions it is best to have separate measurements of M_s vs T. Unfortunately, we are not aware of any data on a composition close to that of our sample. The closest we found was for $Tb_{14}Fe_{86}$ reported by Mimura *et al.*[2] Figure 9 shows the results of mean-field model calculations on $(Tb_{13}Fe_{87})_{93}Ar_7$ along with the above $M_s(T)$ data (O's). The ×'s represent $\beta\theta_k$ for our sample with $\beta = 2500$. They fall slightly below $M_{Fe}(T)$ curve but since our sample has less iron than the one for which the curve was calculated, this is expected. The general behaviors of the theoretical and experimental results, however, are in good agreement.

The above conclusions give weight to the underlying assumptions of the mean-field model in Ref. 7, particularly the postulate that some of the iron atoms in the amorphous RE-TM alloys are antiferromagnetically coupled to their neighboring iron atoms. More data is required, however, for a substantive verification of the model.

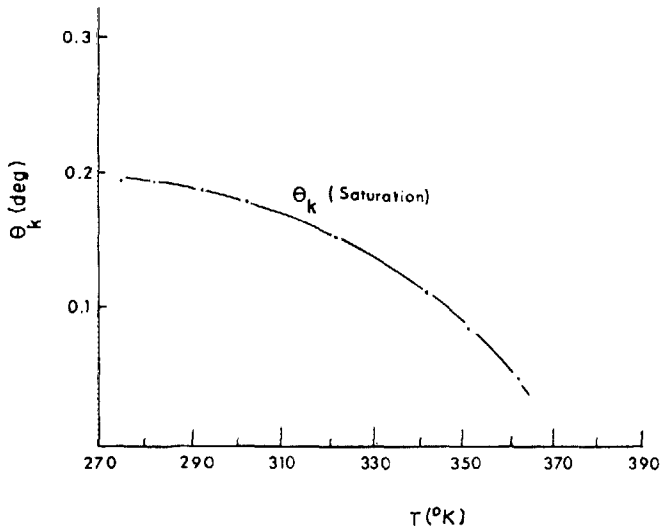

FIG. 8. Kerr rotation angle vs temperature for a 1124-Å-thick sample of $Tb_{16.1}Fe_{77.7}Cu_{6.2}$. Sweep frequency = 0.1 Hz, H_{max} = 1.7 kOe.

IV. MEASUREMENTS OF MAGNETIC ANISOTROPY

Perhaps the most important property of amorphous RE-TM alloys for magneto-optical storage applications is the existence of uniaxial magnetic anisotropy perpendicular to the plane of the films. The energy associated with this magnetic anisotropy can be expressed as

$$E_K(\phi) = K_1 \sin^2\phi + K_2 \sin^4\phi + \cdots, \tag{9}$$

where ϕ is the angle of deviation of the magnetization vector from the normal to the plane of the film and K_1, K_2, ··· are anisotropy energy constants. The uniaxial nature of anisotropy is responsible for the absence of terms with odd powers of ϕ in Eq. (9). Now consider a thin film of amorphous RE-TM alloy with its magnetization saturated to M_s in the perpendicular direction. If an external magnetic field H is applied in the plane of the sample, the magnetization will assume a new orientation in which the angle of M_s with the normal to the plane is ϕ_0, as shown in Fig. 10. To determine ϕ_0 we must write the total magnetic energy as a function of ϕ and minimize it. The energy is usually the sum of external field energy, demagnetizing energy, and the anisotropy energy, and can be expressed as

$$E(\phi) = -HM_s \sin\phi + 2\pi M_s^2 \cos^2\phi + K_1 \sin^2\phi + K_2 \sin^4\phi + \cdots. \tag{10}$$

Let us define x, α, and β as follows:

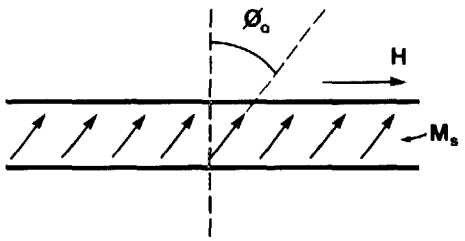

FIG. 10. Magnetization of a thin film with perpendicular anisotropy in the presence of an externally applied in-plane magnetic field H.

$$x = \cos \phi_0,$$
$$\alpha = (K_1/M_s) - 2\pi M_s,$$
$$\beta = K_2/M_s.$$

Then minimization of $E(\phi)$ in Eq. (10) yields the following equation for the calculation of x:

$$4\beta^2 x^6 - 4\beta(\alpha + 3\beta)x^4 + (\alpha + 2\beta)(\alpha + 6\beta)x^2 - (\alpha + 2\beta)^2 + (H/2)^2 = 0. \quad (11)$$

In deriving Eq. (11) we have ignored higher-order terms in the expression of anisotropy energy and retained only the first two terms. Equation (11) is a third-order polynomial equation in x^2 and can be solved to yield x vs H curves. Of the three solutions, the acceptable one is the one that minimizes the total energy $E(\phi_0)$. We will return to this equation after the following description of the experiment.

The experimental procedure for evaluating the anisotropy energy is as follows. The sample is first saturated in the perpendicular direction and then placed in the gap region of a 2-pole magnet where a sinusoidal magnetic field with frequency $f = 0.1$ Hz and amplitude $H_{max} = 17$ kOe is applied in the plane of the sample. The magnetization is monitored by the polar Kerr effect in a system similar to the one shown in Fig. 1. A typical plot of the MO signal vs H is shown in Fig. 11. At $H = 0$ the magnetization is perpendicular to the plane of the sample and the Kerr rotation angle is largest. As the field increases the magnetization vector moves away from the normal and the Kerr angle, being proportional to the perpendicular component of magnetization, decreases. If the field were strong enough the signal would eventually drop to zero, but in our experiment at $H = H_{max}$ the signal has only dropped by 8%, as can be seen from Fig. 11 in which the curve is normalized by the signal from hysteresis loop measurements. The result is thus a curve of $x = \cos \phi_0$ vs H.

It is now easy to find the parameters α and β by matching the solution of Eq. (11) with the experimental data. Let us first assume the simplest model for anisotropy energy and set $K_2 = 0$. Figure 12 shows the experimental data from Fig. 11, represented here by O's and two curves obtained from

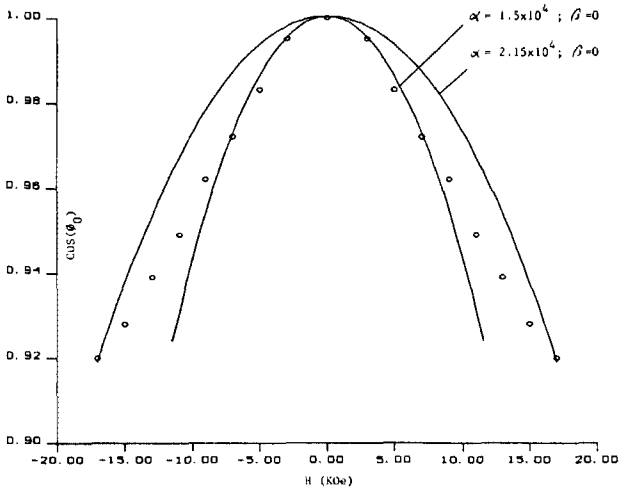

FIG. 12. Comparison between theoretical and experimental results when only the first-order term ($K1$) is included in the model.

Eq. (11), one with $\alpha = 1.5 \times 10^4$ and the other with $\alpha = 2.15 \times 10^4$. ($\beta = 0$ for both curves.) The first curve has the correct curvature around $H = 0$ but is a poor approximation at larger H. The second curve gives the correct value for $\cos \phi_0$ at $H = H_{max}$ but its curvature around $H = 0$ is unacceptable. It is thus clear that the first term in Eq. (9) is not sufficient for the explanation of the observed behavior. Figure 13 shows a good match between the experimental data and the theoretical model assuming $\alpha = 1.25 \times 10^4$, $\beta = 2.75 \times 10^4$. If the mean field model of Fig. 5 is assumed to give the correct value for M_s then at $T = 23$ °C we must have $M_s = 115$ emu/cc, $K_1 = +1.5 \times 10^6$ erg/cc, and $K_2 = +3.2 \times 10^6$ erg/cc. Whether higher-order terms should be included in the expression for anisotropy energy is a question that cannot be answered by our experiment at this point; a more powerful magnet is required to move the magnetization vector further away from its easy axis. The existence of these terms, however, would not affect the values of K_1 and K_2 that were found above in a significant way since the influence of the higher order terms on the curve is mainly at the tails.

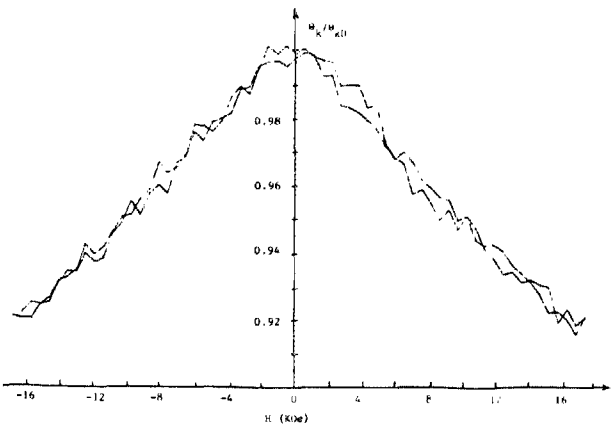

FIG. 11. Normalized values of the polar Kerr magneto-optic effect vs the (in-plane) applied field H for a $Tb_{28.3}Fe_{71.7}$ sample at room temperature. The sweep frequency f is 0.1 Hz.

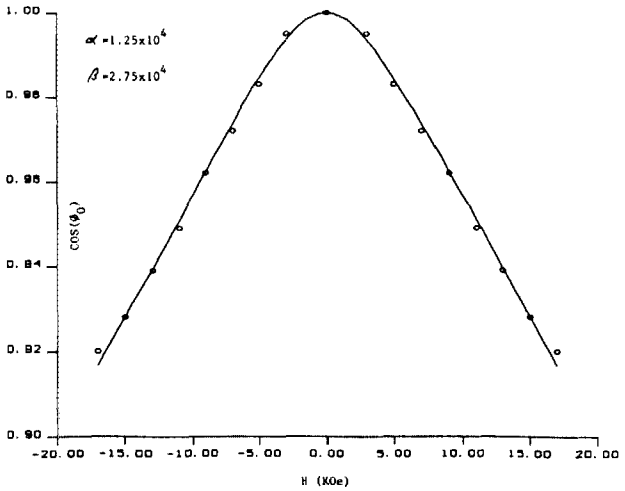

FIG. 13. Comparison between theoretical and experimental results when both the first- and the second-order terms ($K1$ and $K2$) are included in the model.

V. CONCLUDING REMARKS

We have reported on measurements of the polar Kerr effect, coercivity, and magnetic anisotropy in amorphous Tb_xFe_{1-x} alloys and compared these results with theoretical models. This work must now be extended in several directions. First, the temperature range of measurements must be enlarged to include lower temperatures. This would allow a better comparison with the mean-field theory and provide further information about coercivity at low temperatures. Second, the time dependence of magnetization reversal at fields close to the sample's coercivity must be studied for a better understanding of the reversal process. Third the measurements of anisotropy constants must be performed over a range of temperatures to provide further information about the nature of magnetic anisotropy. We are currently working on these problems and hope to report our results in the near future.

ACKNOWLEDGMENTS

Thanks are due to Dr. Alan Bell of IBM's San Jose Research Laboratories for providing the TbFe samples. We have also had many stimulating discussions with Dr. David Treves of the Weizmann Institute of Technology and would like to thank him for his interest in this work. This work has been supported in part by the National Science Foundation Grant No. ECS-8307928.

[1]P. Chaudhari, J. J. Cuomo, and R. J. Gambino, Appl. Phys. Lett. **22**, 337 (1973).
[2]Y. Mimura, N. Imamura, and T. Kobayashi, IEEE Trans. Magn. **12**, 779 (1976).
[3]Y. Mimura, N. Imamura, T. Kobayashi, A. Okada, and Y. Kushiro, J. Appl. Phys. **49**, 1208 (1978).
[4]R. P. Freese, R. N. Gardner, T. A. Rinehart, D. W. Siitari, and L. H. Johnson, Proc. Soc. Photo Instrum. Eng. (SPIE) **529**, 6 (1985).
[5]M. H. Kryder, W. H. Meiklejohn, and R. E. Skoda, Proc. Soc. Photo Instrum. Eng. (SPIE) **420**, 236 (1983).
[6]M. Mansuripur, G. A. N. Connell, and J. W. Goodman, J. Appl. Phys. **53**, 4485 (1982).
[7]M. Mansuripur, M. F. Ruane, and M. N. Horenstein, Proc. Soc. Photo Instrum. Eng. (SPIE), **529**, 25 (1985).
[8]K. Ohashi, H. Tsuji, S. Tsunashima, and S. Uchiyama, Jpn. J. Appl. Phys. **19**, 1333 (1980).